Long term time dependent frequency analysis of chaotic waves in the weakly magnetized spherical Couette system

Ferran Garcia, Martin Seilmayer, André Giesecke, Frank Stefani

Helmholtz-Zentrum Dresden-Rossendorf, Bautzner Landstraße 400, D-01328 Dresden, Germany

Abstract

The long therm behavior of chaotic flows is investigated by means of time dependent frequency analysis. The system under test consists of an electrically conducting fluid, confined between two differentially rotating spheres. The spherical setup is exposed to an axial magnetic field. The classical Fourier Transform method provides a first estimation of the time dependence of the frequencies associated to the flow, as well as its volume-averaged properties. It is however unable to detect strange attractors close to regular solutions in the Feigenbaum as well as Newhouse-Ruelle-Takens bifurcation scenarios. It is shown that Laskar's frequency algorithm is sufficiently accurate to identify these strange attractors and thus is an efficient tool for classification of chaotic flows in high dimensional dynamical systems. Our analysis of several chaotic solutions, obtained at different magnetic field strengths, reveals a strong robustness of the main frequency of the flow. This frequency is associated to an azimuthal drift and it is very close to the frequency of the underlying unstable rotating wave. In contrast, the main frequency of volume-averaged properties can vary almost one order of magnitude as the magnetic forcing is decreased. We conclude that, at the moderate differential rotation considered, unstable rotating waves provide a good description of the variation of the main time scale of any flow with respective variations in the magnetic field.

Keywords: Frequency Analysis, Chaos, Magnetohydrodynamics

1. Introduction

The magnetized spherical Couette (MSC) system -a liquid metal within two differentially rotating spheres subject to a magnetic field- represents one of the fundamental problems for studying three-dimensional magnetohydrodynamic (MHD) instabilities (Hollerbach and Skinner [25], Hollerbach [24], Gissinger et al. [17], Kaplan [28], Garcia and Stefani [13]). The coupled effects of rotation, magnetic fields and spherical geometry, are indeed common in a wide range of processes occurring in celestial objects (Dormy and Soward [9], Moffatt and Dormy [35]), including the generation of the Sun's (Rüdiger [41]) and the Earth's magnetic fields (Jones [27]), or the transport mechanisms in accretion disks around black holes, stars, and protoplanetary disks (Ji and Balbus [26]). The latter have been interpreted in terms of the magnetorotational instability MRI (Balbus and Hawley [3]) which is nowadays considered the best explanation.

Starting with the work by Balbus and Hawley [3] the occurrence of the MRI has been studied in great detail including numerical and experimental work. Experimental investigations of the MRI were conducted at the Helmholtz-Zentrum Dresden-Rossendorf (HZDR) using the GaInSn liquid metal alloy within two rotating cylinders (Stefani et al. [46, 47], Seilmayer et al. [43]), and in Maryland (Sisan et al. [44]) with liquid sodium in spherical geometry. The latter experiment by Sisan et al. [44] motivated the recent numerical studies of Hollerbach [24] and Gissinger et al. [17] which, however, did not interpret the observed instabilities as MRI but as typical instabilities in magnetized spherical Couette (MSC) flows.

To shed light onto this controversy, the HEDGEHOG experiment (Hydromagnetic Experiment with Differentially Gyrating sphEres HOlding GaInSn) has been designed, at HZDR, to describe three-dimensional magnetohydrodynamic instabilities, which are related to the hydrodynamic jet instability, the return flow instability and the Kelvin-Helmholtz-like Shercliff layer instability (see Kasprzyk et al. [29] and the references therein). These instabilities have been studied in the past (e. g. Hollerbach [24], Gissinger et al. [17], Travnikov et al. [49], Kaplan [28]) by means of direct numerical simulations (DNS) of the MSC system, and their spatio-temporal symmetries and nonlinear dynamics have been recently described in terms of bifurcation and dynamical systems theory by Garcia and Stefani [13] and Garcia et al. [15, 16]. We refer to the introductory sections of these latter studies for a detailed summary and references on the numerical studies in the field.

The MSC system is $\mathbf{SO}(2)\times\mathbf{Z}_2$-equivariant, i. e., invariant by azimuthal rotations and reflections with respect to the equatorial plane, and thus a rich variety of nonlinear dynamics is expected (Crawford and Knobloch [6]) thanks to flow bifurcations occurring as the parameters Re (the Reynolds number measuring rotation rates) and Ha (the Hartmann number measuring magnetic field strength) are varied. Bifurcations occurring in systems with symmetry have been largely studied in the past (e. g. Crawford and Knobloch [6], Rand [40], Golubitsky et al. [19], Golubitsky and Stewart [18]). In the particular case of the

MSC system at moderate Re = 10^3 and Ha < 80, the numerical continuation of rotating waves, the theoretical description of modulated rotating waves and the appearance of complex waves and chaotic flows have been recently presented in the studies of Garcia and Stefani [13], Garcia et al. [15], and Garcia et al. [16], respectively. The present study extends these previous works by analyzing the long term behavior of the flows, with special focus on the estimation of the main time scales involved in chaotic flows. The numerical approach relies on a time dependent frequency spectrum analysis of very long time series, including global as well as local flow properties. Laskar's algorithm (Laskar [30], Laskar et al. [33], Laskar [31]), implemented in the SDDSToolkit (Borland et al. [5]), provides a useful tool for an accurate determination of the fundamental frequencies of a time series. Moreover, the study of the time dependent spectrum provides an estimation of the diffusion of the orbit in the phase space (Laskar [32]) and thus can be used to identify chaotic flow behaviour and to study global dynamics. There exist other even more accurate algorithms for the determination of fundamental frequencies, for instance those based on collocation methods described in Gómez et al. [20, 21] and the references therein, which have been used successfully as dynamical indicators. The idea of the analysis of the time-frequency dependence is common (see for instance the work by Djurović and Rubezić [8] or the very recent comparison in Varanis et al. [50]) to assess the chaotic behavior of a nonlinear system.

We recall that for a more complete description of chaos the computation of the so called Lyapunov characteristic exponents LCE (Oseledec [38], Benettin et al. [4], Grappin and Léorat [22]) must be performed and that for this purpose time series tools are available (e. g. Hegger et al. [23]). The latter are based on phase space reconstruction using the method of delays (Takens [48]) and require the adjustment of several parameters such as the embedding dimension or the time delay. A comprehensive analysis of methods for computing LCE, including those based on direct time integrations of the evolution equations and those based on time series, has been recently performed in Awrejcewicz et al. [1] for simple systems. In addition, the study of Awrejcewicz et al. [1] provides a description of the dynamics in terms of Fourier spectra and Gauss wavelets. In a subsequent study (Awrejcewicz et al. [2]) the comparison was extended to a system with $O(10^2)$ degrees of freedom illustrating main problems and difficulties of LCE estimation from a time series. In comparison with those techniques, Laskar's analysis can be applied in a more straightforward manner and only requires to control the accuracy of the obtained frequencies.

With the present study we demonstrate the applicability of Laskar's algorithm, a highly accurate tool for the determination of fundamental frequencies, for identifying chaotic motions in a dissipative dynamical system with a large number $\sim O(10^5)$ of degrees of freedom, due to the spatial discretization of partial differential equations. This is demonstrated for the first time in the context of an MHD problem in spherical geometry. In addition, the study is based on very long time evolutions (more than one order of magnitude larger than the previous studies in the MSC context) which is a challenging task given the dimension of the problem. With the analysis of the time dependent spectrum for two different routes to chaos, the main result found is a strong robustness of the temporal scale associated to an azimuthal flow drift, even for highly oscillatory chaotic flows.

The structure of the paper is as follows: In § 2 the problem and the numerical method used to integrate the model equations are formulated, and the data used for the spectral analysis is described. In § 3 a study of the accuracy for the frequency determination and the set-up for the time dependent spectra is provided. The results are discussed in § 4, considering the Feigenbaum (Feigenbaum [12]) as well as Newhouse-Ruelle-Takens (Newhouse et al. [36]) routes to chaos, and finally in § 5 the paper closes with a discussion on the main results obtained.

2. The model and methods

In the HEDGEHOG experiment a liquid metal (GaInSn) fills the gap between two spheres of radius r_i and r_o with $\chi = r_i/r_o = 0.5$. The inner sphere is rotating with constant velocity Ω around the vertical axis $\hat{\mathbf{e}}_\mathbf{z}$ while the outer is at rest. In addition, an axial magnetic field of amplitude B_0 is applied to the system, see Fig. 1, and insulating boundary conditions are considered for the magnetic field outside the fluid region (e. g. Hollerbach and Skinner [25]).

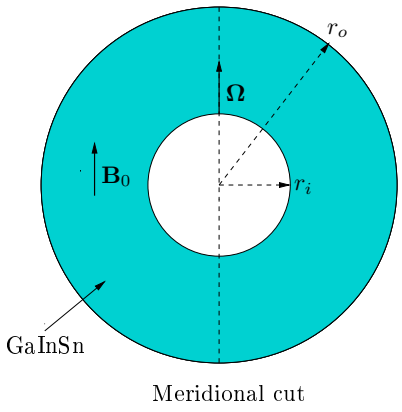

Figure 1: Geometrical configuration of the magnetized spherical Couette (MSC) problem.

The mathematical formulation of the problem relies on the inductionless approximation of the Navier-Stokes and induction equations (Hollerbach and Skinner [25]). Considering η as the magnetic diffusivity, ν as the kinematic viscosity, and $d = r_o - r_i$, the inductionless approximation remains valid when the magnetic Reynolds number Rm = $\Omega r_i d/\eta$ is small, Rm $\ll$ 1. In case of the HEDGEHOG experiment the GaInSn eutectic alloy (Plevachuk et al. [39]) has very low magnetic Prandtl number Pm = $\nu/\eta \sim O(10^{-6})$ and the values for the Reynolds numbers are moderate Re = $\Omega r_i d/\nu \sim 10^3$. This means that Rm = PmRe $\sim 10^{-3}$ and thus the inductionless approximation is valid.

By scaling the length, time, velocity and magnetic field with $d = r_o - r_i$, d^2/ν, $r_i\Omega$ and B_0, respectively, the equations of

motion become

$$\partial_t \mathbf{v} + \mathrm{Re}\,(\mathbf{v}\cdot\nabla)\,\mathbf{v} = -\nabla p + \nabla^2\mathbf{v} + \mathrm{Ha}^2(\nabla\times\mathbf{b})\times\hat{\mathbf{e}}_\mathbf{z}, \quad (1)$$

$$0 = \nabla\times(\mathbf{v}\times\hat{\mathbf{e}}_\mathbf{z}) + \nabla^2\mathbf{b}, \quad (2)$$

$$\nabla\cdot\mathbf{v} = 0, \quad \nabla\cdot\mathbf{b} = 0. \quad (3)$$

where p is the dimensionless pressure containing all the potential forces, $\mathbf{v}$ is the velocity field and $\mathbf{b}$ is the magnetic field perturbation of the axially applied field $\mathbf{B} = \hat{\mathbf{e}}_\mathbf{z} + \mathrm{Rm}\,\mathbf{b}$. The no-slip ($v_r = v_\theta = v_\varphi = 0$) and constant rotation ($v_r = v_\theta = 0$, $v_\varphi = \sin\theta$) conditions are imposed on the boundary at $r = r_o$ and $r = r_i$, respectively. For the magnetic field the exterior regions are assumed to be insulating, as it is the case for the HEDGEHOG experiment. The magnetic field boundary conditions are formulated in terms of the spherical harmonics (see Hollerbach and Skinner [25] for full details). The system is governed by 3 non-dimensional numbers:

$$\mathrm{Re} = \frac{\Omega r_i d}{\nu}, \quad \mathrm{Ha} = \frac{B_0 d}{\sqrt{\rho\nu\mu_0\eta}}, \quad \text{and} \quad \chi = \frac{r_i}{r_o},$$

with μ_0 being the magnetic permeability for free-space and ρ being the density of the fluid. The parameters selected for the present study, $\chi = 0.5$, $\mathrm{Re} = 10^3$ and $\mathrm{Ha} < 6$, are in accordance with the typical operating parameters of the HEDGEHOG experiments, in which $\eta = 0.35, 0.5$, $\mathrm{Re} \in [10^3, 10^4]$ and $\mathrm{Ha} < 10^3$.

The pseudo-spectral method for the numerical solution of the governing equations is briefly described in the following. For full details we refer to Garcia and Stefani [13] and references therein. The divergence-free velocity field $\mathbf{v} = \nabla\times(\Psi\mathbf{r}) + \nabla\times\nabla\times(\Phi\mathbf{r})$ is expressed as a sum of the toroidal, Ψ, and poloidal, Φ, potentials, with $r = r\,\hat{\mathbf{e}}_\mathbf{r}$ being the position vector. For the radial coordinate a collocation method on a Gauss–Lobatto mesh of N_r points is employed. For the angular coordinates the scalar potentials are expanded in spherical harmonic series up to degree $L_{\max}$ and order $M_{\max} = L_{\max}$:

$$(\Psi,\Phi)(t,r,\theta,\varphi) = \sum_{l=0}^{L_{\max}}\sum_{m=-l}^{l}(\Psi,\Phi)_l^m(r,t)Y_l^m(\theta,\varphi), \quad (4)$$

with $\Psi_l^{-m} = (\Psi_l^m)^*$ and $\Phi_l^{-m} = (\Phi_l^m)^*$, $(\cdot)^*$ meaning complex conjugation. By choosing $\Psi_0^0 = \Phi_0^0 = 0$ the two scalar potentials are uniquely determined. We recall that $Y_l^m(\theta,\varphi) = P_l^m(\cos\theta)\mathrm{e}^{im\varphi}$ is the spherical harmonic function with P_l^m being the normalized associated Legendre functions of degree l and order m. High order implicit-explicit backward differentiation formulas IMEX–BDF (Garcia et al. [14]) are used for the time integration. The nonlinear terms are considered explicitly to avoid the solution of a nonlinear system at each time step. An explicit treatment of the Lorenz force term facilitates the implementation of the linear solver, but may lead to smaller time integration steps (Δt) in comparison with an implicit treatment. However, this is not critical as moderate Ha are considered in the present study.

Two different diagnostics are considered for the analysis of the DNS. First, the time series of the radial velocity v_r picked up at the point $(r,\theta,\varphi) = (r_i + 0.5d, \pi/8, 0)$, which is a local measure that reflects the time scales of the flow. Second, the time series of the volume-averaged kinetic energy K, defined as

$$K = \frac{1}{2\mathcal{V}}\int_\mathcal{V}\mathbf{v}\cdot\mathbf{v}\,dv, \quad (5)$$

with $\mathcal{V}$ being the volume of the shell and $\mathbf{v}$ being the velocity field, provides a global measure. Instead of considering K for the total flow, we compute the kinetic energy K_m defined by only employing the spherical harmonic amplitudes Ψ_l^m and Φ_l^m with order m and degree l satisfying $|m| \le l \le L_{\max}$. This provides an idea on the distribution of kinetic energy among the different azimuthal modes m. For the flows we are analyzing (see Garcia et al. [16]) there exists an $m_{\max}$ with $\overline{K}_{m_{\max}} \gg \overline{K}_m$, $1 \le m \le L_{\max}$, and $m \ne m_{\max}$, with the over-line representing a time average. We note that then the flow will exhibit $m_{\max}$ vortices. If in addition the flow has m_d-fold azimuthal symmetry, then it is unaffected by azimuthal rotations multiples of $2\pi/m_d$ and the spherical harmonic amplitudes with azimuthal wave numbers being multiples of m_d are the only nonzero ones in Eq. (4). Notice that if the azimuthal symmetry is $m_d = 1$ all the spherical harmonics amplitudes are considered.

3. Frequency analysis

For an accurate determination of the fundamental frequencies of a time series, Laskar's method (Laskar [31]) of numerical analysis of fundamental frequencies (NAFF) is employed. This method, implemented in the SDDSToolKit (Borland et al. [5]), involves a von-Hann-window and FFT together with a numerical optimization of the difference between the signal and exponential functions of time. Concretely, given a time series $(t_i, p(t_i))$, $t_i = t_{i-1} + \Delta t$, $i = 1,\ldots,N$ of a quasiperiodic function p, defined on a time interval $[0,T]$, Laskar's algorithm provides the decomposition of $p(t)$ on the basis $\mathrm{e}^{-\mathrm{i}f_j t}$ which is nonorthogonal on a finite time window, computing the frequencies f_j, $j = 1,...,M$, with an iterative algorithm. It first starts by finding the maximum term of the FFT of the time series. The corresponding frequency, f, is refined to obtain f_1 by maximizing the power spectrum

$$\int_0^T p(t)\mathrm{e}^{-\mathrm{i}ft}H(t)dt,$$

where $H(t) = 1 + \cos(\pi t/T)$ is the von-Hann-window filter (helps to reduce the coupling effect of other frequencies). Once f_1 is found, the corresponding term is removed from the time series and the process is repeated to find f_2. After finding each f_j we note that since the basis functions $\mathrm{e}^{-\mathrm{i}f_j t}$ are not orthogonal an intermediate step of orthogonalization (Gauss algorithm) is required to compute the amplitudes. The algorithm stops whenever the new frequency f_k satisfies $|f_k - f_j| < 1.5\times 2\pi/T$, for any $j < k$, which corresponds to the band limitation of an FFT with a von-Hann-window filter.

3.1. Accuracy estimation

In order to estimate the accuracy of Laskar's algorithm for the determination of the frequency with the largest amplitude,

a rotating (also travelling) wave (RW) with azimuthal symmetry $m = 4$ and rotating frequency ω is considered (i. e. a periodic flow whose temporal dependence can be described as $u(t, r, \theta, \varphi) \equiv u(r, \theta, \varphi - \omega t)$). The parameters of this RW are $\chi = 0.5$, Re $= 10^3$ and Ha $= 3.7766571$.

Because a RW is a periodic orbit, it can be obtained by means of a continuation method (Garcia and Stefani [13]) and its rotating frequency estimated up to a prescribed tolerance. Specifically, we solve a nonlinear system which determines a single RW defined by (u, τ, p), with $\tau = 2\pi/(m\omega)$ being the period, at a parameter $p =$ Ha. The system is

$$H(u, \tau, p) = \begin{pmatrix} u - \phi(\tau, u, p) \\ g(u) \\ m(u, \tau, p) \end{pmatrix} = 0, \tag{6}$$

where $\phi(\tau, u, p)$ is a solution of Eqs. (1)-(3) at time τ and initial condition u for fixed p. The condition $g(u) = 0$ is selected to fix the undetermined phase of the RW and $m(u, \tau, p)$ is the pseudo-arclength condition of the continuation method. This system is solved by employing a Newton-Krylov procedure with tolerance 10^{-8}. The method is matrix-free and so does not require the explicit computation of the Jacobian $D_{(u,\tau,p)}H(u, \tau, p)$, but only its action on a given vector (see Garcia and Stefani [13] for full details).

Once the RW with $m = 4$ at Ha $= 3.7766571$ has been obtained with the Newton-Krylov procedure, a direct time integration of the MSC equations is performed to obtain the time series of the radial velocity v_r picked up at the point $(r, \theta, \varphi) = (r_i + 0.5d, \pi/8, 0)$ for which Laskar's algorithm is applied subsequently. This particular location allows to measure the meridional circulation of the flow at high latitudes. Because the radial velocity amplitude is significant on a wide region in the bulk of the shell (see e. g. Fig. 12 in Garcia et al. [16]) the results should not depend on the measurement position. We have checked this by also considering the point $(r, \theta, \varphi) = (r_i + 0.85d, 3\pi/8, \pi/2)$. The step for the time integration is the same, $\Delta t = 5 \times 10^{-6}$, as that used for the time integration within Newton's method. We note that this Δt provides enough accuracy (we have used a 4th order time integration scheme) with errors less than 10^{-8} because otherwise Newton's method does not converge. The use of high order time integration methods is recommended when a highly accurate time integration is required (Garcia et al. [14]).

Newton's method (with tolerance 10^{-8}) gives $\omega = 138.09097$ which corresponds to the frequency $f = m\omega/2\pi = 87.91144$ whereas Laskar's algorithm result is $f = 87.91145$ for $T \geq 0.3$, T being the time interval of the time series from which the frequency f has been computed. The sampling time interval is $\Delta t_{\text{samp}} = 10^{-4}$ dimensionless time units. The case yields $f = 87.91068$ for $T = 0.1$, but $f = 87.91151$ for $T = 0.2$. By decreasing $\Delta t_{\text{samp}} = 10^{-5}$ the same results are obtained, but for $\Delta t_{\text{samp}} = 2 \times 10^{-4}$ the accuracy is degraded to $f = 87.91167$ even for $T = 20$. The accuracy provided by Laskar's algorithm is estimated to be $O(1/T^3)$ (e. g. Laskar [32]) contrasting the $O(1/T)$ estimation for the classical FFT. In the case of computing f with FFT, with $\Delta t_{\text{samp}} = 10^{-4}$, we obtain $f = 87.9000$ for $T = 20$ and $f = 87.91666$ for $T = 60$, meaning that a time window $T \geq 60$, which is large for a simple periodic time series, has to be considered in the FFT to detect changes in the frequency which are below 1%. As it will be evidenced latter, this makes the FFT unpractical to detect the chaotic flows studied here.

3.2. Time dependent frequency spectrum

Our analysis is based on very long time integrations up to a final time $T_f = 100$ (in dimensionless time units), which corresponds to 2×10^7 time integration steps ($\Delta t = 5 \times 10^{-6}$). This is a challenging task because of the large dimension $n \sim O(10^5)$ of the ODE system due to the spatial discretization of the MSC governing equations.

Given a flow initial condition $u \in \mathbb{R}^n$, which will be detailed in the next section, the frequency f of maximum amplitude is computed from a time window $[t, t + T] \subset [0, T_f]$ of the time series. According to Laskar [32] this provides the map

$$\begin{aligned} F_T : \mathbb{R}^n \times \mathbb{R} &\longrightarrow \mathbb{R} \\ (u, t) &\longrightarrow f(u, t) \end{aligned}$$

which can be used for the analysis of the diffusion of the orbit $u \in \mathbb{R}^n$ with respect to time, and thus infer the regular or chaotic behavior of the orbit. If the flow is quasiperiodic F_T is a constant function of time whereas for chaotic flows F_T varies indicating the diffusion of the orbit in phase space.

As noticed in Laskar [32] the frequencies are computed up to a certain accuracy, ϵ_f, depending on the solution u and the time window T. For the case of a rotating wave, we have shown in the previous section that this accuracy for Laskar's algorithm is about $\epsilon_f = 10^{-5}$, even for very small time windows $T = 0.3$. For the analysis of quasiperiodic and chaotic flows we may assume slightly larger discrepancies ϵ_f. Then, flows are considered to be regular if F_T is constant within ϵ_f of accuracy, otherwise to be chaotic. Following Laskar [32] we also estimate the instantaneous diffusion rate as $\delta F_T(u, t) = |F_T(u, t + T) - F_T(u, t)|$. The diffusion of the orbit is nonzero, i. e. the flow is nonregular, when $\delta F_T(u, t) > \epsilon_f$. For the analysis of the flows presented in this study we evaluate $F_T(u, t)$ at the time instants $t_i = 0.1(i - 1) \leq T_f - T$ and $\delta F_T(u, t)$ at the same time instants but for $t_i \leq T_f - 2T$.

For the analysis, either with Laskar's or FFT algorithm, of all the time series considered in this study the setup is the following: A sampling time step $\Delta t_{\text{samp}} = 10^{-4}$ has been used as it provides the best accuracy from the estimation given in Sec. 3.1. In addition, several sizes of the time window $T = 1$, 2.5, 5, 10, 20 and 40 have been considered to check that the results do not depend on the particular choice of the time window size.

4. Results: Analysis of chaotic flows

Several flow realizations that correspond to two different routes to chaos (Eckmann [10]) are studied in this section. The first scenario is in accordance with the Feigenbaum route (Feigenbaum [12]) in which chaotic flows are developed after a sequence of period doubling bifurcations. The second scenario

corresponds to the Newhouse-Ruelle-Takens route (Newhouse et al. [36]) in which strange attractors develop from a sequence of Hopf bifurcations giving rise to quasiperiodic flows. These two routes have been already identified and described in the recent study of Garcia et al. [16] devoted to the MSC problem in a parameter regime corresponding to the radial jet instability, in which the magnetic effects are weak. The specific problem parameters are $\chi = 0.5$, $\mathrm{Re} = 10^3$ and $\mathrm{Ha} < 4$. The description of Garcia et al. [16], based on the study of bifurcation diagrams and Poincaré sections, evidenced both scenarios. Concretely, for the Feigenbaum scenario, the distance between the successive period bifurcation points was used in Garcia et al. [16] to estimate the Feigenbaum constant within 5% of accuracy. In the case of the Newhouse-Ruelle-Takens scenario, the different bifurcations giving rise to two and three-frequency flows, before the appearance of chaos, were identified in Garcia et al. [16].

For the present study we are interested in the description of long term behavior of solutions belonging to these two scenarios which give rise to chaotic flows. We select three different flows at each of the routes (Newhouse-Ruelle-Takens and Feigenbaum) presented in Garcia et al. [16] and perform the analysis summarized in Sec. 3.2 to estimate the diffusion of the corresponding orbits and the time variation of the main frequency f (that with maximum amplitude) either of the time series of the radial velocity or the time series of the $m = 2$ volume-averaged kinetic energy (already defined in Sec.2). These time series are obtained from direct numerical simulations as described in Garcia et al. [16]. The spatial resolution requirements, $N_r = 40$ and $L_{\max} = 84$, for solving the MSC equations have been already validated in Garcia and Stefani [13] and, as commented in Sec. 3.1, high order time integration is employed to obtain accurate time series.

4.1. Feigenbaum scenario

This section focuses on chaotic flows originating from a period-doubling cascade of quasiperiodic flows with two fundamental frequencies (i. e. two-tori) and with $m = 2$ azimuthal symmetry. A detailed analysis of this scenario was performed in Garcia et al. [16]. In this latter study the Feigenbaum iterates $\delta_i = (\mathrm{Ha}_{i+1} - \mathrm{Ha}_i)/(\mathrm{Ha}_{i+2} - \mathrm{Ha}_{i+1})$, with $\mathrm{Ha}_1 = 3.491$, $\mathrm{Ha}_2 = 3.423$, $\mathrm{Ha}_3 = 3.4073$, and $\mathrm{Ha}_4 = 3.4039$ being the successive period-doubling bifurcation points, have been estimated to be $\delta_1 = 4.33$ and $\delta_2 = 4.62$, in reasonable agreement with the Feigenbaum constant $\delta = 4.6692$.

For the analysis of the time dependence of frequency spectra in the Feigenbaum route a quasiperiodic flow with two fundamental frequencies at $\mathrm{Ha} = 3.425$ and two chaotic flows at $\mathrm{Ha} = 3.4$ and $\mathrm{Ha} = 0.7$ are selected. Notice that for $\mathrm{Ha} = 3.425$ a period-doubling bifurcation has already occurred and that the chaotic flow at $\mathrm{Ha} = 3.4$ is close to the onset of chaos (the last period doubling found is at $\mathrm{Ha}_4 = 3.4039$). We have selected this regular solution to compare the results with the two other chaotic flows along the Feigenbaum route. The regular and chaotic flows at $\mathrm{Ha} = 3.425$ and $\mathrm{Ha} = 3.4$ have $m = 2$ azimuthal symmetry whereas the azimuthal symmetry of the chaotic flow at $\mathrm{Ha} = 0.7$ is $m = 1$. As studied in Garcia et al. [16], the chaotic nature of the flows remains by decreasing Ha from $\mathrm{Ha} = 3.4$. The flows close to $\mathrm{Ha} = 0$ are strongly oscillatory with $m_{\max} = 2$.

Figure 2 displays the time series of the radial velocity v_r and the volume averaged kinetic energy K_2 of the $m = 2$ component of the flow (see Sec. 2) for the regular and chaotic flows at $\mathrm{Ha} = 3.425$ and $\mathrm{Ha} = 0.7$, respectively, in case of the Feigenbaum scenario. For the 2-frequency solution (panels (a) and (b)), the time series of v_r exhibits a quasiperiodic behavior whereas the time series of K_2 remains periodic, showing the period-doublings. This is because the solution is a modulated rotating wave (Rand [40], Garcia et al. [15]) and one of the frequencies is associated with the rigid rotation (azimuthal drift) of the flow patterns. By azimuthally averaging the flow, only the frequency of modulation is observed. The time series of the chaotic flow at $\mathrm{Ha} = 0.7$ (panels (c) and (d)) exhibit a clear chaotic behavior, but the small temporal scale (associated to the azimuthal drift shown in panel (a)) of the radial velocity still prevails.

Figure 3(a,b) illustrates the analysis of the radial velocity time series of the regular solution at $\mathrm{Ha} = 3.425$, corresponding to a quasiperiodic flow with two fundamental frequencies (a modulated rotating wave, see Garcia et al. [15]) and with azimuthal symmetry $m = 2$. Figure 3(a) provides $f(t)$ computed using a time window of $T = 5, 10, 20, 40$ (the higher the amplitude of the oscillations the smaller the time window) for the regular wave. As f is computed from the time series of v_r it corresponds to the frequency of the azimuthal drift of the wave. A very weak time dependence is observed which damps out by increasing T. For $T \geq 10$ the relative oscillations of f are less than 10^{-5} and the time difference $\delta f(t) = |f(t+T) - f(t)| \lesssim 10^{-4}$ (see Fig. 3(b)). We assume this values to be valid for classifying this flow as regular, considering an accuracy $\epsilon_f = 10^{-4}$ for the frequency determination. We note that although a value of

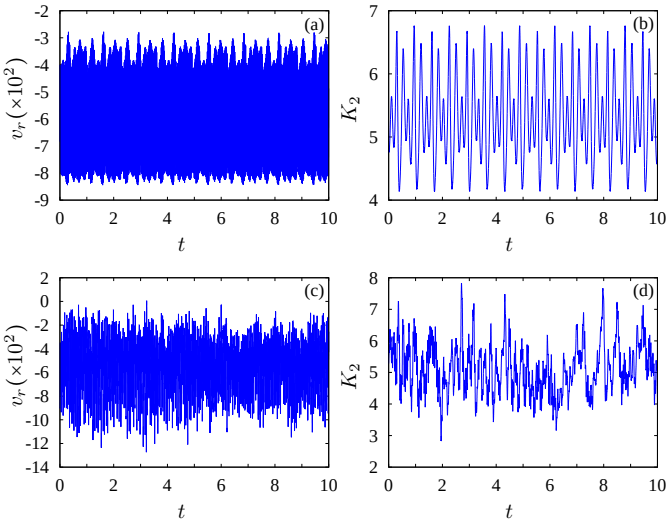

Figure 2: (a,c) The time series of the radial velocity picked up at the point $(r, \theta, \varphi) = (r_i + 0.5d, \pi/8, 0)$. (b,d) The time series of the volume averaged kinetic energy of the $m = 2$ component of the flow. (a,b) are for a regular flow with two fundamental frequencies at $\mathrm{Ha} = 3.425$, and (c,d) are for a chaotic flow at $\mathrm{Ha} = 0.7$.

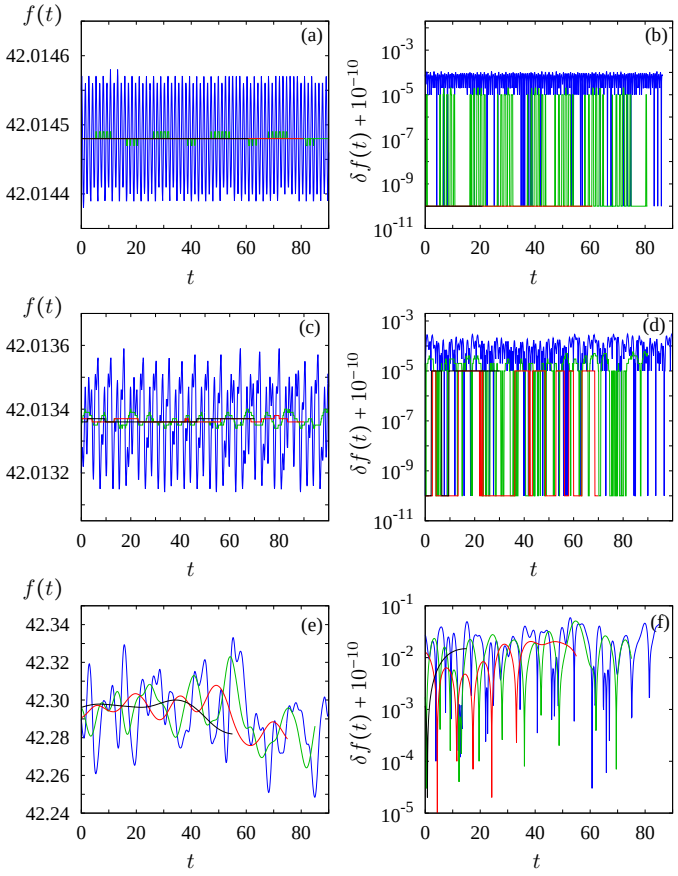

Figure 3: Time dependent frequency spectrum based on Laskar algorithm (SDDSToolKit). The time series correspond to the radial velocity picked up at the point $(r, \theta, \varphi) = (r_i + 0.5d, \pi/8, 0)$. (a,c) Frequency with maximum amplitude versus time. (b,d) Time difference $\delta f(t) = |f(t+T) - f(t)|$ versus time (logscale). Different colors denote different lengths of the time series (blue $T = 5$, green $T = 10$, red $T = 20$ and black $T = 40$). Panels (a,b) are for a regular solution at Ha = 3.425, panels (c,d) are for a chaotic solution at Ha = 3.4, and panels (e,f) for a chaotic solution at Ha = 0.7.

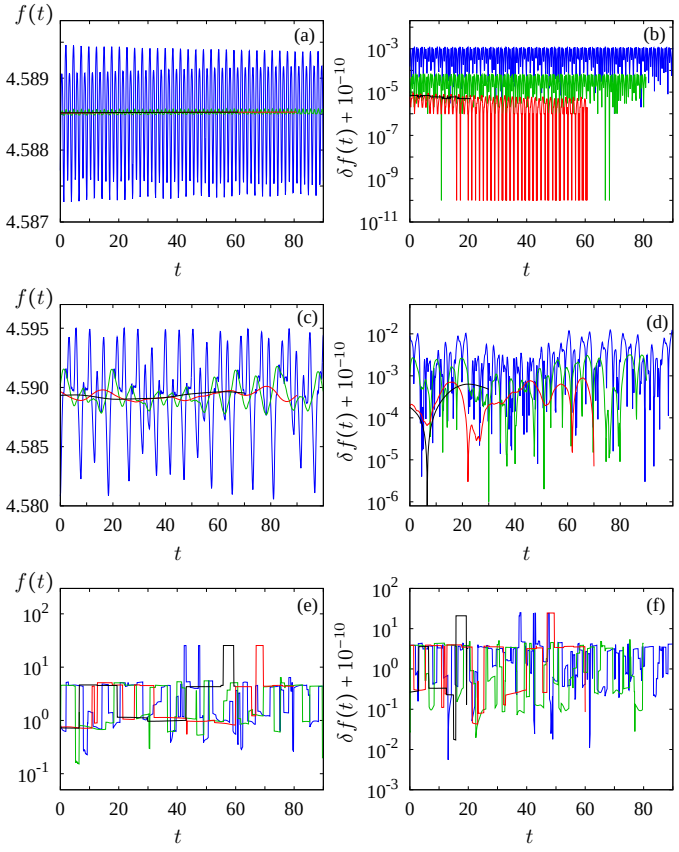

Figure 4: Time dependent frequency spectrum based on Laskar algorithm (SDDSToolKit). The time series corresponds to the volume averaged kinetic energy of the $m = 2$ component of the flow. (a,c) Frequency with maximum amplitude versus time. (b,d) Time difference $\delta f(t) = |f(t+T) - f(t)|$ versus time (logscale). Different colors denote different lengths of the time series (blue $T = 5$, green $T = 10$, red $T = 20$ and black $T = 40$). Panels (a,b) are for a regular solution at Ha = 3.425, panels (c,d) are for a chaotic solution at Ha = 3.4, and panels (e,f) for a chaotic solution at Ha = 0.7.

$\epsilon_f = 10^{-5}$ was achieved in Sec. 3.1 in the case of a rotating wave (i. e. a periodic orbit), the regular solution now has 2 fundamental frequencies which may increase the uncertainty in frequency determination. We notice, however, that for $T \geq 20$ the value of f is constant within $\epsilon_f = 10^{-7}$.

Because the flow at Ha = 3.4 is close to the origin of period-doubling chaos, the range of variation of f and δf is small but relevant, providing a chaotic signature (see Fig. 3(c,d)). For the largest time window considered, $T = 40$, the difference value is $\delta t \leq 10^{-5}$, clearly larger than $\epsilon_f = 10^{-7}$. The values for f and δf for the chaotic flow at Ha = 0.7 (shown in Fig. 3(e,f)) are more pronounced but still remain small. For instance, f oscillates around its mean value with less than 1% for all considered time windows T, which indicates the robust character of the frequency associated to the azimuthal drift, even for this highly oscillatory flow.

The analysis for the volume averaged kinetic energy of the $m = 2$ component of the flow, summarized in Fig. 4, provides a better measure of chaotic behavior as the value of δf and the interval of variation of f increase by one order of magnitude with respect to the analysis of the radial velocity. As a consequence different diffusion rates of the orbit emerge within the phase space so that volume-averaging provides a better description of these chaotic flows. We note that for the regular solution a slightly noticeable transient can be identified on Fig. 4(a,b), because of the regular solution at $Ha = 3.425$ being close to the second period doubling bifurcation at $\mathrm{Ha}_2 = 3.423$, so that long transients can be expected. Nevertheless values of $\delta f < 10^{-5}$, for $T \geq 20$, are obtained, which supports our assumption of $\epsilon_f = 10^{-5}$ for the largest time windows. The value of δf is clearly larger than this threshold (for $T \geq 20$) when analyzing the chaotic solution at Ha = 3.4 (see Fig. 4(d)).

In contrast to the previous chaotic flows, the description for the highly oscillatory flow at Ha = 0.7 is substantially different (see Fig. 4(e,f)). In this case, the frequency f spans around two orders of magnitude and the values of δf raise up to $O(10)$, accounting for a wide range of temporal scales in volume-averaged quantities. We recall that this was not the case for the main frequency of the radial velocity displayed in Fig. 3(e,f). To highlight the differences between the main time scales of the flow and those of volume-averaged quantities the time de-

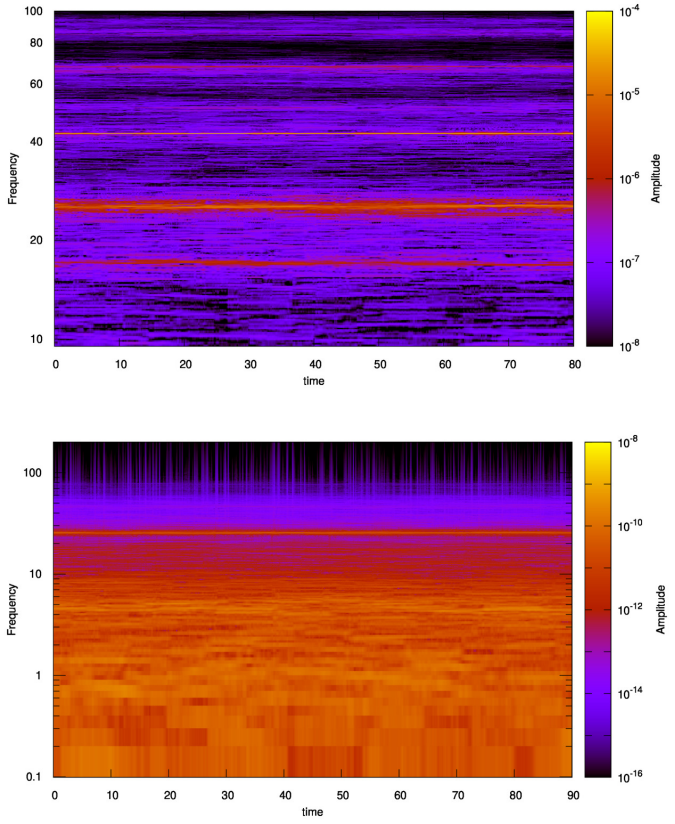

Figure 5: Time dependent frequency spectrum based on FFT on a time window $T = 10$ for the chaotic flow at Ha = 0.7. The time series correspond to (a) the radial velocity picked up at the point $(r, \theta, \varphi) = (r_i + 0.5d, \pi/8, 0)$ and (b) the volume averaged kinetic energy of the $m = 2$ component of the flow. For the volume-averaged kinetic energy, the frequency with maximum amplitude varies on a broad range $f \in (0.1, 100)$. In contrast, for the time series corresponding to the local measurement (radial velocity) the frequency with maximum amplitude remains constant ($f = 42.3$) in the whole time range.

pendent spectrum based on FFT is provided in Fig. 5. With the FFT analysis and a time window of $T = 10$ the frequency of maximum amplitude of the flow remains constant at $f = 42.3$ whereas a broad band of main frequencies is obtained in case of the volume-averaged kinetic energy of the $m = 2$ component of the flow.

We note that the FFT analysis for the chaotic solution at Ha = 3.4 provides constant frequencies $f = 42$ and $f = 4.6$ for v_r and K_2, respectively. We recall that, as for Laskar's analysis, the time windows $T = 5, 10, 20$, and 40, and sampling time step $\Delta t_{\text{samp}} = 10^{-4}$ are considered. Then, FFT analysis is unable to detect the chaotic nature for solutions with Ha being close to the onset of chaos. This is because for these flows δf (see either Fig. 3(c,d) or Fig. 4(c,d)) is smaller than the accuracy $O(1/T) > 0.02$ achieved with the FFT. This will be further evidenced on the next section dedicated to the Newhouse-Ruelle-Takens scenario.

4.2. Newhouse-Ruelle-Takens scenario

One quasiperiodic flow with three fundamental frequencies at Ha = 0.7, and two chaotic flows at Ha = 0.67 and Ha = 0.63 are considered for the Newhouse-Ruelle-Takens scenario. They belong to the same branch as described in Garcia et al. [16] with $m = 1$ azimuthal symmetry and $m_{\max} = 2$. Bifurcation diagrams of two and three frequency solutions and eventually chaotic flows, characteristic of the Newhouse-Ruelle-Takens scenario, were analyzed in Garcia et al. [16] for Ha < 1 in terms of Poincaré sections. We show in this section that the appearance of chaos can be also evidenced by investigating the time dependence of the main frequency obtained with Laskar's procedure.

Figure 6(a) displays $f(t)$ for the regular wave with 3 fundamental frequencies at Ha = 0.7. In comparison with the regular solution of the Feigenbaum scenario, the variation of the frequency with maximum amplitude f and the value of δf is clearly larger for a fixed time window T. The regular solution for the Feigenbaum scenario has two fundamental frequencies whereas that of the Newhouse-Ruelle-Takens scenario has three. This may be the reason for the smaller value of ϵ_f achieved for the regular solution in case of the Feigenbaum route.

For the chaotic flows at Ha = 0.67 (Figs. 6(c,d)) and Ha =

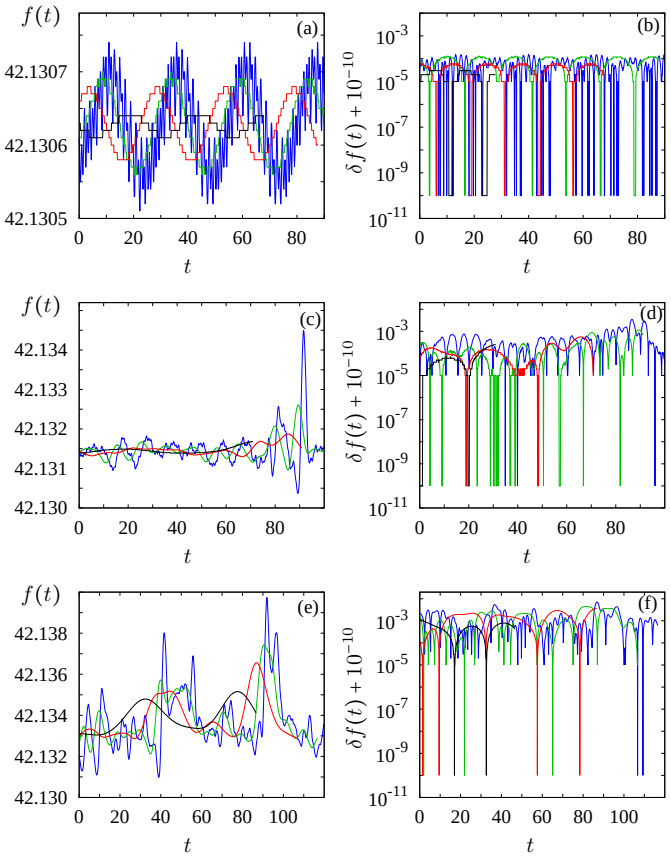

Figure 6: Time dependent frequency spectrum based on Laskar's algorithm (SDDSToolKit). The time series correspond to the radial velocity picked up at the point $(r, \theta, \varphi) = (r_i + 0.5d, \pi/8, 0)$. (a,c,e) Frequency with maximum amplitude versus time. (b,d,f) Time difference $\delta f(t) = |f(t + T) - f(t)|$ versus time (logscale). Different colors denote different length of the time series (blue $T = 5$, green $T = 10$, red $T = 20$ and black $T = 40$). Panels (a,b) are for a regular solution at Ha = 0.7, panels (c,d) are for a chaotic solution at Ha = 0.67, and panels (e,f) are for a chaotic solution at Ha = 0.63.

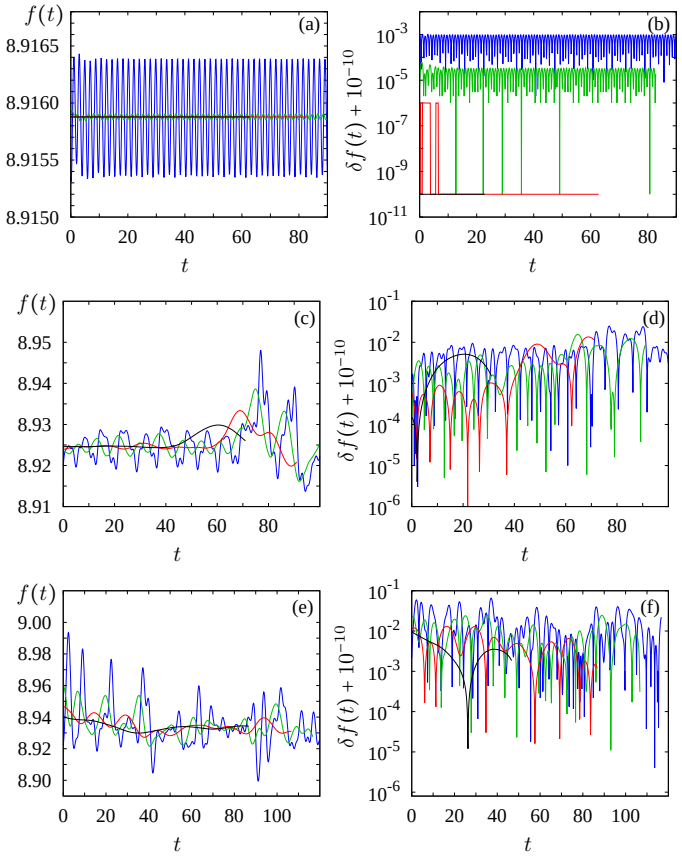

Figure 7: Time dependent frequency spectrum based on Laskar's algorithm (SDDSToolKit). The time series correspond to the volume averaged kinetic energy of the $m = 2$ component of the flow. (a,c,e) Frequency f with maximum amplitude versus time. (b,d,f) Time difference $\delta f(t) = |f(t+T) - f(t)|$ versus time (logscale). Different colors denote different length of the time series (blue $T = 5$, green $T = 10$, red $T = 20$ and black $T = 40$). Panels (a,b) are for a regular solution at Ha = 0.7, panels (c,d) are for a chaotic solution at Ha = 0.67, and panels (e,f) are for a chaotic solution at Ha = 0.63.

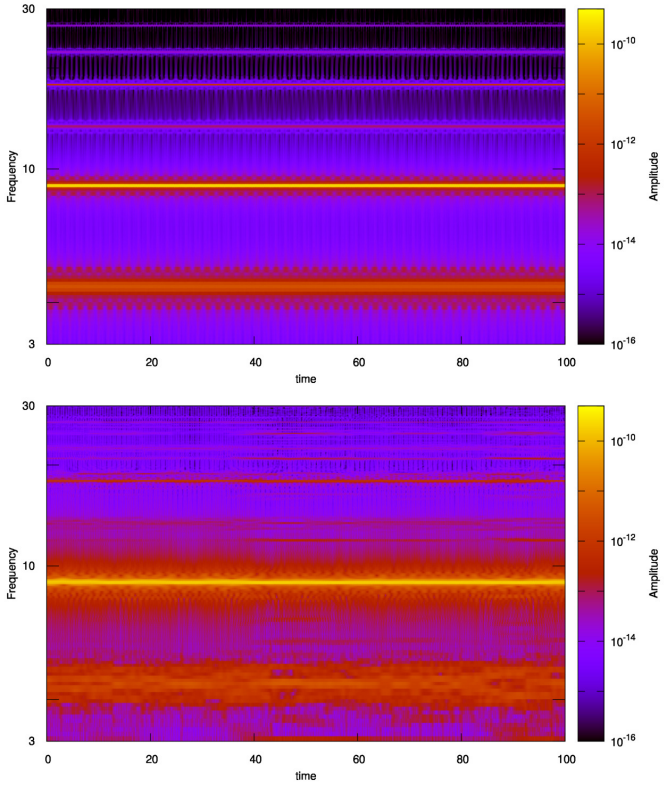

Figure 8: Time dependent frequency spectrum based on FFT on a time window $T = 10$. The time series correspond to the volume averaged kinetic energy of the $m = 2$ component of the flow. (a) Three frequency quasiperiodic flow at Ha = 0.74 and (b) Chaotic flow at Ha = 0.63. The frequency with maximum amplitude remains constant in the whole time range and is $f = 8.9$, for both Ha = 0.74 and Ha = 0.63, and thus it does neither reveal the chaotic behavior for Ha = 0.63 nor it reflects the dependence of f on Ha.

0.63 (Figs. 6(e,f)) the variation of f and the value of δf is significant and the amplitude of their oscillations is growing with time. For the chaotic flows the value of δf is at least one order of magnitude larger than for the regular flow, although it is still small, indicating slow diffusion of the orbit in the phase space. Indeed, as for chaotic flows in the Feigenbaum scenario, the range of variation of f is narrow which indicates a nearly uniform azimuthal drift for these chaotic flows.

As in the Feigenbaum case, the frequency description considering the $m = 2$ volume-averaged kinetic energy, which is summarized in Fig. 7, is even more clear than that corresponding to the radial velocity. For the chaotic flows at Ha = 0.67 and Ha = 0.63 the maximum value of δf is larger than 10^{-2}, but the corresponding maximum value is smaller than 10^{-5} for the regular solution at Ha = 0.7. In addition, and in agreement with the Feigenbaum scenario, for the chaotic flows at Ha = 0.67 and Ha = 0.63 the value of δf is significantly larger when considering a volume-averaged measure than when considering a measure of the flow itself. As discussed in the previous section this indicates two very different diffusion rates of the orbit in the phase space.

To highlight the superiority of Laskar's algorithm with respect to the common FFT the moving FFT frequency spectrum of the volume-averaged kinetic energy of the $m = 2$ component of the flow is presented in Fig. 8(a,b). The top plot corresponds to a regular flow at Ha = 0.74, i. e. at a Hartmann number larger than the regular flow at Ha = 0.7 presented in this section, whereas the bottom plot corresponds to the chaotic flow at Ha = 0.63 with larger variation of f in Fig. 7. Although for the chaotic flow the moving spectra exhibit some irregular bands around secondary frequencies, the frequency of largest amplitude remains constant to $f = 8.9$ at Ha = 0.63 (also Ha = 0.67), which is the same value obtained for the regular flow, at significantly different Ha = 0.74. For the figure a time window of $T = 10$ is used, however, for the other values of $T = 5, 20$, and 40, the results remain basically unchanged. This confirms the results presented in the previous section, i. e., for chaotic flows with Ha near the onset of chaos a highly accurate determination of the frequency of maximum amplitude is required to detect the chaotic nature of these flows because the time fluctuations of this frequency can be very small.

Table 1: Mean frequency $\overline{f}$ with maximum amplitude, and its absolute difference $\varepsilon_f = f_{\max} - f_{\min}$. The time dependent frequency of maximum amplitude f is computed on a time window T from the time series of the radial velocity picked up at the point $(r, \theta, \varphi) = (r_i + 0.5d, \pi/8, 0)$. This frequency is associated to the drifting behaviour of the waves. The superscript $*$ indicates a regular solution, otherwise the solution is chaotic.

		Newhouse-Ruelle-Takens			Feigenbaum		
T	Ha	0.7^*	0.67	0.63	3.425^*	3.4	0.7
1	$\overline{f}$	42.13	42.13	42.13	42.01	42.01	40
1	ε_f	3×10^{-2}	4×10^{-2}	6×10^{-2}	4×10^{-2}	5×10^{-2}	20
2.5	$\overline{f}$	42.131	42.13	42.13	42.014	42.013	42
2.5	ε_f	4×10^{-3}	10^{-2}	2×10^{-2}	4×10^{-3}	6×10^{-3}	17
5	$\overline{f}$	42.1303	42.132	42.134	42.0144	42.0131	42.29
5	ε_f	2×10^{-4}	4×10^{-3}	9×10^{-3}	2×10^{-4}	5×10^{-4}	8×10^{-2}
10	$\overline{f}$	42.1304	42.132	42.134	42.01448	42.01337	42.29
10	ε_f	10^{-4}	2×10^{-3}	5×10^{-3}	2×10^{-5}	6×10^{-5}	6×10^{-2}
20	$\overline{f}$	42.13057	42.1316	42.134	42.014481	42.01337	42.29
20	ε_f	9×10^{-5}	6×10^{-4}	4×10^{-3}	0	2×10^{-5}	3×10^{-2}
40	$\overline{f}$	42.13082	42.1313	42.134	42.014481	42.01336	42.295
40	ε_f	3×10^{-5}	3×10^{-4}	2×10^{-3}	0	10^{-5}	2×10^{-2}

Table 2: Mean frequency $\overline{f}$ with maximum amplitude, and its absolute difference $\varepsilon_f = f_{\max} - f_{\min}$. The time dependent frequency of maximum amplitude f is computed on a time window T from the time series of the volume averaged kinetic energy of the $m = 2$ component of the flow. This frequency is associated to the modulation behaviour of the waves. The superscript $*$ indicates a regular solution, otherwise the solution is chaotic.

		Newhouse-Ruelle-Takens			Feigenbaum		
T	Ha	0.7^*	0.67	0.63	3.425^*	3.4	0.7
1	$\overline{f}$	8.92	8.9	8.9	4.5	4.5	4
1	ε_f	7×10^{-2}	2×10^{-1}	2×10^{-1}	10^{0}	10^{0}	25
2.5	$\overline{f}$	8.92	8.93	8.9	4.59	4.59	25
2.5	ε_f	3×10^{-2}	8×10^{-2}	10^{-1}	5×10^{-2}	8×10^{-2}	3
5	$\overline{f}$	8.916	8.93	8.94	4.589	4.59	25
5	ε_f	10^{-3}	3×10^{-2}	9×10^{-2}	2×10^{-3}	10^{-2}	3
10	$\overline{f}$	8.91589	8.93	8.93	4.58856	4.589	6
10	ε_f	9×10^{-5}	2×10^{-2}	4×10^{-2}	9×10^{-5}	4×10^{-3}	3
20	$\overline{f}$	8.915878	8.93	8.93	4.58852	4.589	25
20	ε_f	2×10^{-6}	10^{-2}	2×10^{-2}	2×10^{-5}	10^{-3}	3
40	$\overline{f}$	8.9158783	8.926	8.93	4.588518	4.5893	25
40	ε_f	0	6×10^{-3}	10^{-2}	2×10^{-6}	6×10^{-4}	4

5. Summary and conclusions

The present study is based on very long high order time integrations of the MSC equations, with a discretized system of $O(10^5)$ degrees of freedom. Specifically the DNS, on a spherical shell with an aspect ratio $\chi = 0.5$, cover 100 viscous time units at a Reynolds number $\mathrm{Re} = 10^3$. This represents around 1.6×10^4 inner sphere rotation periods, which is a value two orders of magnitude larger than the achieved by previous studies in the field (e. g. Hollerbach [24], Kaplan [28]).

The time series of local (the radial velocity at a point inside the shell) and global (a volume-averaged kinetic energy) measures have been analyzed using Laskar's algorithm for the determination of fundamental frequencies (Laskar [31]). The accuracy of the method (down to 10^{-7} in relative values) is estimated using a periodic flow (a rotating wave) from which the frequency can be obtained using a Newton-Krylov procedure (Garcia and Stefani [13]).

Several regular and chaotic flows are selected for the analysis. At first one regular and two chaotic flows from the Feigenbaum scenario (Feigenbaum [12]) are investigated. Similarly, one regular and two chaotic flows representing the Newhouse-Ruelle-Takens scenario (Newhouse et al. [36]) are selected as well. These two routes to chaos were confirmed in Garcia et al. [16] by computing the corresponding solution branches and performing a Poincaré section analysis. In this paper we extend the previous study of Garcia et al. [16] by investigating time dependent frequency spectra. Following the work of Laskar [32], the frequency of maximum amplitude f is computed on several time windows to study the time dependence of $f(t)$ and $\delta f(t) = |F(t + T) - f(t)|$. This helps to confirm the existence of chaos and to estimate the diffusion of the orbit in the phase space.

The results are summarized in Tables 1 and 2 and in figure 9. From the tables as well as from the figure it can be concluded

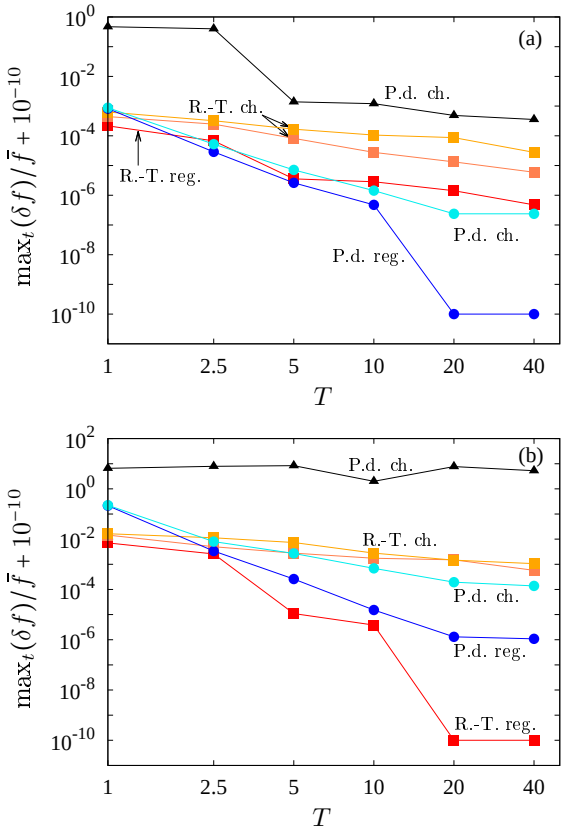

Figure 9: Relative difference $\max(\delta f(t))/\bar{f},\ 0 \le t \le 100$, with $\delta f(t) = |f(t+T) - f(t)|$, versus the time window T for the Newhouse-Ruelle-Takens (R.-T., full squares), Feigenbaum (P.d., full circles and triangle) chaos (ch.) scenarios. Regular (reg.) flows for the R.-T. and P.d. scenarios are considered as well. The time series correspond to (a) the volume averaged kinetic energy of the $m = 2$ component of the flow and (b) the radial velocity picked up at the point $(r, \theta, \varphi) = (r_i + 0.5d, \pi/8, 0)$.

that a minimum time window of $T = 5$ viscous time units should be used to obtain reliable results that allow an identification of chaos. This is because for small time windows, $T \le 5$, the fluctuations of $f(t)$ (either measured by ε_f, or by $\max(\delta f(t))/\bar{f},\ 0 \le t \le 100$,) observed for the regular solutions are of the same order of magnitude than those observed for the chaotic flows.

The range of variation of the frequency, $\varepsilon_f = f_{\max} - f_{\min}$, for the local measure (radial velocity; table 1) is significantly smaller than that for the global one (volume-averaged kinetic energy; table 2). This is also true when considering the relative difference $\max(\delta f(t))/\bar{f},\ 0 \le t \le 100$, displayed in Fig. 9. The latter evidences different diffusion rates in the phase space as the measured frequencies are obtained from different components (total or volume-averaged) of the flow.

The classical Fourier transform is not accurate enough to detect small frequency changes over time $|\delta f| < 2/T = 10^{-2}$ for the considered observation windows. This motivates the use of an optimization method like Laskar's, which finds the most probable frequency due to a Newton method and (successive) single mode elimination. The result is a more precise estimate of the dominant frequency; we have shown that for the Feigenbaum and Newhouse-Ruelle-Takens scenarios this is key for identifying the onset of those chaotic flows, which exhibit small variations of f.

We stress that a rigorous confirmation of a strange attractor would require the computation of the leading Lyapunov characteristic exponent (LCE) (e. g. Eckmann and Ruelle [11]). This is beyond of the scope of this study as it would require long time runs of the MSC system coupled with its first variationals (see Benettin et al. [4] for details), which is a challenging computational task. We note that the validity for applying time dependent frequency analysis in chaotic systems has been already tested by Laskar et al. [33] and Gómez et al. [20] against the computation of LCE. The latter studies already noted that frequency analysis seems to require a shorter time evolution than the computation of LCE to detect a strange attractor, which is a key issue for large dimensional systems.

As commented in the introductory section there exist tools which are able to estimate LCE from a time series (see Hegger et al. [23] and references therein) but these tools require to tune several input parameters (e. g. Awrejcewicz et al. [2]) and thus are more sophisticated than Laskar's method, which only depends on the precision of the frequency computation. This is also true for other time series methods such as those based on wavelet transforms (Daubechies [7], Meyer [34]) which decompose the signal into a set of orthogonal basis functions, localized in the time-frequency domain. Wavelet methods have been successfully used for the analysis of chaotic solutions by Staszewski, W. J. and Worden, K. [45] (also by Sarma et al. [42] for a magnetized plasma experiment) but they require to select the wavelet type, filter and length, which are key parameters to be tuned to obtain an accurate analysis (see Zhang et al. [51] in the case of neuron activity signals).

A remarkable result is that for all types of flows, the frequency corresponding to the mean azimuthal drift (inferred from the radial velocity) remains nearly constant and only oscillates less than 0.2% with respect to its mean value giving rise to very small ($< 10^{-2}$) diffusion rates. This is especially surprising in the case of the highly oscillatory chaotic flow from the Feigenbaum scenario at Ha = 0.7, as the frequency corresponding to the main time scale of a volume-averaged quantity can vary more than one order of magnitude. We have tested other chaotic flows in the same branch as well as all other classes of chaotic flows found by Garcia et al. [16] and the results are similar. The main conclusion is that the azimuthal drift behaviour of flows at moderate Reynolds number $\mathrm{Re} = 10^3$ is strongly robust, even for highly oscillatory chaotic flows.

As found in Garcia et al. [16], for each class of flows with azimuthal mode $m_{\max}$, mostly contributing to the kinetic energy, the frequency associated with the azimuthal drift was very close to that of the unstable rotating wave with azimuthal symmetry $m_{\max}$, at the same Hartmann number. With the present analysis we have demonstrated that this frequency is indeed quite robust even when considering long time integrations. Thus, unstable rotating waves provide a good description of the main time scale of the MSC flow at moderate $\mathrm{Re} = 10^3$ and $\mathrm{Ha} < 6$.

The present study sheds light on the analysis of future HEDGEHOG experiments at $\mathrm{Re} = 10^3$ and $\mathrm{Ha} < 4$, which

corresponds to the radial jet instability regime. The experiment is designed to effectively work for low Ha (see Kasprzyk et al. [29]) assuming an error of about 1% in the selection of the parameters (see also Ogbonna et al. [37]). The analysis of the DNS points to the difficulty of distinguishing regular and chaotic flows in the experiment using time dependent spectral analysis since highly accurate computation of the main frequency (provided by Laskar's algorithm) is required.

The key issue is that chaotic DNS exhibit small time fluctuations of the main frequency of the flow velocity, which require large enough observation windows of $T \geq 5$, to be distinguishable from the intrinsic numerical fluctuations associated to the approximation of the frequency, which are also present in the case of regular solutions. With a kinematic viscosity of the eutectic alloy GaInSn of $\nu = 3.4 \times 10^{-3}\mathrm{cm}^2\mathrm{s}^{-1}$ (Plevachuk et al. [39]) the time scale in seconds is $t^* = td^2/\nu = 5.96 \times 10^3 t$, t being the dimensionless time and the gap width $d = r_o - r_i = 9\ \mathrm{cm} - 4.5\ \mathrm{cm} = 4.5\ \mathrm{cm}$. Thus $T \geq 5$ represents around 8 hours of the HEDGEHOG experiment, which is almost the limit of a typical experimental run (up to 10 hours) because of the degradation of the signal quality (Ogbonna et al. [37]). This means that observational time windows of maximum size $T \sim 2$ can be considered in the experiment which are impractical for detecting chaotic flows if the analysis of the main frequency obtained from a velocity measurement is performed.

By analyzing the volume-averaged kinetic energy, and not directly the flow velocity, we have shown that the main frequency can vary several orders of magnitude (even for small time windows of $T = 1$) in the case of a chaotic flow belonging to the Feigenbaum scenario at Ha $= 0.7$ (see Table 2). These chaotic flows could be detected in the experiment provided that the time-dependent spectral analysis is performed to a secondary frequency of the flow reflecting the modulation of volume-averaged properties. This can be done within the HEDGEHOG measurement setup as the frequency spectrum can be computed independently for the $m = 0, 1, 2, 3, 4$ and 5 azimuthal wave number components of the flow (see Ogbonna et al. [37] for details). The analysis of the volume-averaged kinetic energy does not work for detecting the onset of chaotic flows if time windows of $T < 5$ are used, neither for the Feigenbaum nor the Newhouse-Ruelle-Takens scenarios.

Acknowledgments

F. Garcia kindly acknowledges the Alexander von Humboldt Foundation for its financial support. This project has also received funding from the European Research Council (ERC) under the European Union's Horizon 2020 research and innovation programme (grant agreement No 787544).

References

[1] J. Awrejcewicz, A.V. Krysko, N.P. Erofeev, V. Dobriyan, M.A. Barulina, and V.A. Krysko. Quantifying chaos by various computational methods. Part 1: Simple systems. *Entropy*, 20(175), 2018.

[2] J. Awrejcewicz, A.V. Krysko, N.P. Erofeev, V. Dobriyan, M.A. Barulina, and V.A. Krysko. Quantifying chaos by various computational methods. Part 2: Vibrations of the Bernoulli–Euler beam subjected to periodic and colored noise. *Entropy*, 20(170), 2018.

[3] S. A. Balbus and J. F. Hawley. A powerful local shear instability in weakly magnetized disks. i- Linear analysis. ii- Nonlinear evolution. *Astrophys. J.*, 376:214–233, 1991.

[4] G. Benettin, L. Galgani, A. Giorgilli, and J. M. Strelcyn. Lyapunov characteristic exponents for smooth dynamical systems and for Hamiltonian systems: A method for computing all of them. *Meccanica*, 15:9–20, 1980.

[5] M. Borland, L. Emery, H. Shang, and R. Soliday, 2017. User's Guide for SDDS Toolkit Version 3.51, It is available on the web at `https://ops.aps.anl.gov/manuals/SDDStoolkit/SDDStoolkit.html`.

[6] J. D. Crawford and E. Knobloch. Symmetry and symmetry-breaking bifurcations in fluid dynamics. *Annu. Rev. Fluid Mech.*, 23(1):341–387, 1991.

[7] I. Daubechies. *Ten Lectures on Wavelets*. SIAM, Philadelphia, 1991.

[8] I. Djurović and V. Rubezić. Chaos detection in chaotic systems with large number of components in spectral domain. *Signal Processing*, 88(9): 2357–2362, 2008.

[9] E. Dormy and A. M. Soward, editors. *Mathematical Aspects of Natural Dynamos*, volume 13 of *The Fluid Mechanics of Astrophysics and Geophysics*. Chapman & Hall/CRC, Boca Raton, FL, 2007. ISBN 978–1-58488-954-0.

[10] J.-P. Eckmann. Roads to turbulence in dissipative dynamical systems. *Rev. Mod. Phys.*, 53(4):643–654, 1981.

[11] J.-P. Eckmann and D. Ruelle. Ergodic theory of chaos and strange attractors. *Rev. Mod. Phys.*, 57(3):617–656, 1985.

[12] M. J. Feigenbaum. Quantitative universality for a class of nonlinear transformations. *J. Stat. Phys.*, 19:25–52, 1978.

[13] F. Garcia and F. Stefani. Continuation and stability of rotating waves in the magnetized spherical Couette system: Secondary transitions and multistability. *Proc. R. Soc. A*, 474:20180281, 2018.

[14] F. Garcia, M. Net, B. García-Archilla, and J. Sánchez. A comparison of high-order time integrators for thermal convection in rotating spherical shells. *J. Comput. Phys.*, 229:7997–8010, 2010.

[15] F. Garcia, M. Seilmayer, A. Giesecke, and F. Stefani. Modulated rotating waves in the magnetized spherical Couette system. *J. Nonlinear Sci.*, 29: 2735–2759, 2019.

[16] F. Garcia, M. Seilmayer, A. Giesecke, and F. Stefani. Chaotic wave dynamics in weakly magnetised spherical Couette flows. *Chaos*, 30(4): 043116, 2020.

[17] C. Gissinger, H. Ji, and J. Goodman. Instabilities in magnetized spherical Couette flow. *Phys. Rev. E*, 84:026308, 2011.

[18] M. Golubitsky and I. Stewart. *The Symmetry Perspective: From Equilibrium to Chaos in Phase Space and Physical Space.* Birkhäuser, Basel, 2003.

[19] M. Golubitsky, V. G. LeBlanc, and I. Melbourne. Hopf bifurcation from rotating waves and patterns in physical space. *J. Nonlinear Sci.*, 10:69–101, 2000.

[20] G. Gómez, J. M. Mondelo, and C. Simó. A collocation method for the numerical fourier analysis of quasi-periodic functions. I: Numerical tests and examples. *Discrete Cont. Dyn. B*, 14(1):41–74, 2010.

[21] G. Gómez, J. M. Mondelo, and C. Simó. A collocation method for the numerical Fourier analysis of quasi-periodic functions. II: Analytical error estimates. *Discrete Cont. Dyn. B*, 14(1):75–109, 2010.

[22] R. Grappin and J. Léorat. Lyapunov exponents and the dimension of periodic incompressible Navier-Stokes flows: numerical measurements. *J. Fluid Mech.*, 222:61–94, 1991.

[23] R. Hegger, H. Kantz, and T. Schreiber. Practical implementation of nonlinear time series methods: The tisean package. *Chaos*, 413, 1999.

[24] R. Hollerbach. Non-axisymmetric instabilities in magnetic spherical Couette flow. *Proc. R. Soc. A*, 465:2003–2013, 2009.

[25] R. Hollerbach and S. Skinner. Instabilities of magnetically induced shear layers and jets. *Proc. R. Soc. A*, 457:785–802, 2001.

[26] H. Ji and S. Balbus. Angular momentum transport in astrophysics and in the lab. *Phys. Today*, 66(8):27–33, 2013.

[27] C. A. Jones. Planetary magnetic fields and fluid dynamos. *Annu. Rev. Fluid Mech.*, 43(1):583–614, 2011.

[28] E. J. Kaplan. Saturation of nonaxisymmetric instabilities of magnetized spherical Couette flow. *Phys. Rev. E*, 89(063016):1–8, 2014.

[29] C. Kasprzyk, E. Kaplan, M. Seilmayer, and F. Stefani. Transitions in a magnetized quasi-laminar spherical Couette flow. *Magnetohydrodynam-*

ics, 53(2):393–401, 2017.

[30] J. Laskar. The chaotic motion of the solar system: A numerical estimate of the size of the chaotic zones. *Icarus*, 88(2):266 – 291, 1990.

[31] J. Laskar. Frequency analysis of a dynamical system. *Celestial Mech. Dyn. Astron.*, 56:191–196, 1993.

[32] J. Laskar. Frequency analysis for multi-dimensional systems. Global dynamics and diffusion. *Physica D*, 67:257–281, 1993.

[33] J. Laskar, C. Froeschlé, and A. Celletti. The measure of chaos by the numerical analysis of the fundamental frequencies. application to the standard mapping. *Physica D*, 56(2):253 – 269, 1992.

[34] Y. Meyer. *Wavelets: Algorithms & Applications*. SIAM, Philadelphia, 1993.

[35] K. Moffatt and E. Dormy. *Self-Exciting Fluid Dynamos*. Cambridge Texts in Applied Mathematics. Cambridge University press, 2019.

[36] S. Newhouse, D. Ruelle, and F. Takens. Occurrence of strange axiom A attractors near quasiperiodic flows on t^m, $m \geq 3$. *Commun. Math. Phys.*, 64:35–40, 1978.

[37] J. Ogbonna, F. Garcia, T. Gundrum, M. Seilmayer, and F. Stefani. Experimental investigation of the return flow instability in magnetic spherical Couette flow. Submitted to Phys. Fluids.

[38] V. I. Oseledec. A multiplicative ergodic theorem: Lyapunov characteristic numbers for dynamical systems. *Trans. Moscow Math. Soc.*, 19:197–231, 1968.

[39] Y. Plevachuk, V. Sklyarchuk, S. Eckert, G. Gerbeth, and R. Novakovic. Thermophysical properties of the liquid Ga-In-Sn eutectic alloy. *J. Chem. Eng. Data*, 59(3):757–763, 2014.

[40] D. Rand. Dynamics and symmetry. Predictions for modulated waves in rotating fluids. *Arch. Ration. Mech. Anal.*, 79(1):1–37, 1982.

[41] G. Rüdiger. *Differential Rotation and Stellar Convection: Sun and Solar-type Stars*. Fluid mechanics of astrophysics and geophysics. Gordon and Breach Science Publishers, 1989.

[42] B. Sarma, S. S. Chauhan, A. M. Wharton, and A. N. S. Iyengar. Continuous wavelet transform analysis for self-similarity properties of turbulence in magnetized DC glow discharge plasma. *Journal of Plasma Physics*, 79 (5):885–891, 2013.

[43] M. Seilmayer, V. Galindo, G. Gerbeth, T. Gundrum, F. Stefani, M. Gellert, G. Rüdiger, M. Schultz, and R. Hollerbach. Experimental evidence for nonaxisymmetric magnetorotational instability in a rotating liquid metal exposed to an azimuthal magnetic field. *Phys. Rev. Lett.*, 113:024505, 2014.

[44] D. R. Sisan, N. Mujica, W. A. Tillotson, Y. M. Huang, W. Dorland, A. B. Hassam, T. M. Antonsen, and D. P. Lathrop. Experimental observation and characterization of the magnetorotational instability. *Phys. Rev. Lett.*, 93:114502, 2004.

[45] Staszewski, W. J. and Worden, K. Wavelet analysis of time-series: Coherent structures, chaos and noise. *Int. J. Bifurcation and Chaos*, 9:455–471, 1999.

[46] F. Stefani, T. Gundrum, G. Gerbeth, G. Rüdiger, M. Schultz, J. Szklarski, and R. Hollerbach. Experimental evidence for magnetorotational instability in a Taylor-Couette flow under the influence of a helical magnetic field. *Phys. Rev. Lett.*, 97:184502, 2006.

[47] F. Stefani, G. Gerbeth, T. Gundrum, R. Hollerbach, J. Priede, G. Rüdiger, and J. Szklarski. Helical magnetorotational instability in a Taylor-Couette flow with strongly reduced Ekman pumping. *Phys. Rev. E*, 80:066303, 2009.

[48] F. Takens. Detecting strange attractors in turbulence. *Lecture Notes in Math.*, 898, 1981.

[49] V. Travnikov, K. Eckert, and S. Odenbach. Influence of an axial magnetic field on the stability of spherical Couette flows with different gap widths. *Acta Mech.*, 219:255–268, 2011.

[50] M. Varanis, J.P.C.V. Norenberg, R.T. Rocha, C. Oliveira, J.M. Balthazar, and A.M. Tusset. A comparison of time-frequency methods for nonlinear dynamics and chaos analysis in an energy harvesting model. *Braz. J. Phys.*, 2020.

[51] Z. Zhang, Q. K. Telesford, C. Giusti, K.O Lim, and D. S. Bassett. Choosing wavelet methods, filters, and lengths for functional brain network construction. *PLoS ONE*, 11(6):e0157243, 2016.